Magnetic iron nanoparticles in carbon nanotubes

Author: Alba Teixidó Villanueva
Facultat de Física, Universitat de Barcelona, Diagonal 645, 08028 Barcelona, Spain.

Advisors: Dr.Javier Tejada Palacios & Jaume Calvo de la Rosa

Abstract: In this work we have studied the magnetic properties of iron nanoparticles mixed with carbon nanotubes. The ZFC-FC curves, M(H) loops and the magnetic relaxation were measured using a SQUID-magnetometer (Superconducting Quantum Interference Detector device). The ZFC and FC processes have been measured with an applied field of 100, 2000, 3000 and 5000 Oe, respectively. The ZFC curves show two peaks which may correspond to two different blocking temperatures. The energy barriers distribution was studied from the derivative of the difference between ZFC and FC curves with respect to temperature . Isothermal hysteresis loops M(H) show a higher coercitivity and irreversability with decreasing temperature. The magnetic relaxation measurements were performed down to 2K.The magnetic viscosity shows a linear dependence with temperature. Moreover we have also measured the complex permittivity in the frequency range of 200 MHz and 20 GHz and real and imaginary components of the magnetic susceptibility between 2-300K when 10 Hz and 1000 Hz frequencies were applied .

I. INTRODUCTION

The research field of carbon nanotubes (CNTs) has received a continuously growing interest since their discovery in 1991 [1]. Carbon nanotubes present interesting properties, such as an excellent thermal conductivity,a high mechanical stress and a large elastic modulus and elastic strain [2].

CNTs mixed with ferromagnetic materials are interesting because carbon media possess magnetic properties,that is why carbon based materials are diamagnetic. While by introducing different kind of NPs we can observe ferromagnetic and paramagnetic behaviour [3].

It is also well known that the properties of materials with nanometric sizes differ from bulk scale. In a bulk ferromagnet we find magnetic domains separated by domain walls, whereas in a nano-micrometric range we have an assembly of magnetic particles displaying a energy barrier distribution.

The aim of this work is to have a fully understanding of the magnetic properties of these materials based upon the existing energy barrier distribution.

II. CHARACTERIZATION OF THE SAMPLE

The sample that we are going to describe is made of iron nanoparticles (NPs) intercalated into CNTs.

X-ray diffraction of the sample was performed for phase identification by using Cu-alpha radiation. The pattern is shown in figure 1. Analyzing the peaks with X'Pert HighScore we can identify three principal phases (table 1). Moreover, the relative intensity of the peaks allows us to obtain the composition by using the Reference Intensity Ratio (RIR) method.

Morphology of the sample was determined using a Scanning Electron Microscopy (SEM). From images obtained from SEM, cubic shapes can be observed which may correspond to an agglomeration of nanotubes with iron particles inside them. The composition and SEM image can be seen in figure 2.

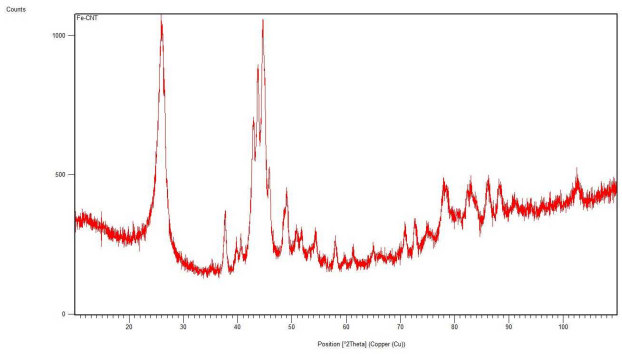

FIG. 1: XRD pattern of Fe-CNT sample

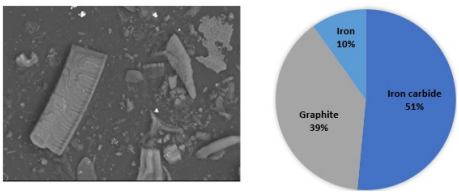

FIG. 2: SEM image of Fe-CNT sample(left) and composition of the sample (right)

Phase	Crystal system	Reference code
Fe	Cubic	01-087-0721
Fe_3C	Orthorhombic	01-072-1110
Carbon	Rhombohedral	01-074-2329

TABLE I: Phase , crystal system and reference code obtained with peak analysis of the sample.

III. THEORETICAL FRAMEWORK

A. Magnetic relaxation

If we consider an ensemble of magnetic particles having different directions and orientations of their easy axis and we apply a magnetic field until the saturation, all their magnetic moments will be oriented in the same direction than the field. When we remove the field, the relaxation process starts. Some particles, having small energy barriers will be able to demagnetize very fast while those particles with larger barrier heights will remain with their magnetic moments oriented along the external magnetic field. The variation of the magnetization with time depends on the transition frequency between the two possible states (considering the case of an uniaxial magnetic anisotropy).

$$\frac{dM}{dt} = -M\Gamma \tag{1}$$

The transition frequency depends on the energy barrier (U), temperature (T) and Boltzmann constant (k_B).

$$\Gamma = \nu \exp\left(-\frac{U}{k_B T}\right) \tag{2}$$

So this can be related with the time that the particle needs to reverse the magnetization. If we have an ensemble of particles, the energy barrier depends on magnetization.

$$U = U_0\left(1 - \frac{M(t)}{K_B T}\right) \tag{3}$$

Finally, we obtain that the magnetization has a logarithmic dependence with time and has a proportionality with temperature.

$$M(t) = M(t_0)\left(1 - \frac{K_B T}{U_0}\ln\left(\frac{t}{t_0}\right)\right) \tag{4}$$

B. Barrier distribution

From the variation with temperature of the difference between ZFC-FC curves it is possible to extract the barrier distribution by using equation (5).

$$g\left(\phi_B(T)\right) = \frac{1}{\alpha}T^{2/3}\frac{dM_{FC-ZFC}}{dT} \tag{5}$$

Where alpha is a constant:

$$\alpha = \frac{MS^2 H\mu 0}{2KB}\frac{1}{3}\left(\frac{6}{\pi}\right)^{1/3}\left(\frac{KB\ln(\frac{\tau m}{\tau 0})}{K}\right)^{1/3} \tag{6}$$

To compute the barrier distribution with our experimental data, we approximate the previous expression (6) .

$$\mathrm{g}(\phi) \propto \mathrm{T}^{2/3}\frac{\Delta(\mathrm{M_{FC}}-\mathrm{M_{ZFC}})}{\Delta T} \tag{7}$$

IV. EXPERIMENTAL

The magnetization was measured using a SQUID magnetometer. This device measures changes in magnetic field using quantum interference coils.

We have used 5 mg of the sample to do the magnetic measurements. We cannot exceed this weight due to the sensitivity of the SQUID, otherwise it would be impossible to record the magnetization due to the high saturation.

The permittivity measurements were taken with *8517B S-Parameter Test Set, 0.045 to 20 GHz* using *85070C DIELECTRIC PROBE KIT* for calibration. We prepared 5 ml of sample. Due to the shortage of the sample, we could not measure higher volumes. We do not have a precise criteria to determine the pressure that we applied between the surface of the sample and the contact of the device , however we take the measurements in function of number of turns of the wheel that lifts up support.

V. RESULTS AND DISCUSSION

A. Hysteresis cycles

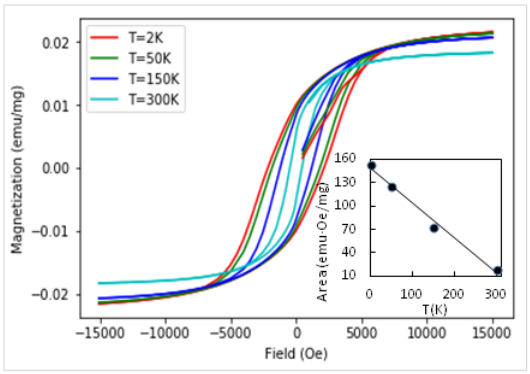

FIG. 3: Hysteresis cycles at different temperatures and the dependence on temperature of area involved in M(H) loops.

The hysteresis cycles at different temperatures are shown in figure 3. The evolution of magnetization shows a narrowing tendency towards higher temperature. Moreover the irreversibility of the loops suggest an energy barrier distribution, due to the progressive thermal activation that allows the jump of energy barriers. On the other hand, we can also observe a linear behaviour above magnetic saturation. The slope shows a linear dependence with temperature and it may correspond to the Curie law indicating a superparamagnetic behaviour due to the existence of very small magnetic particles.

The main magnetostatic parameters can be extracted from the hysteresis magnetization curves , the coercitivity and remanent magnetization. Both present a linear dependence with temperature. At lower temperatures

higher values of coercivity are obtained because thermal energy is reduced. We also calculate the area involved in the M(H) curves (figure 3), which is related with the losses of hysteresis cycle. The area shows a linear dependence with temperature which is in good agreement with the linear dependence of remanent magnetization and coercitivity.

B. ZFC-FC curves

In order to obtain information about energy barriers, we performed ZFC and FC measures to determine the temperature dependent magnetization at different magnetic fields.

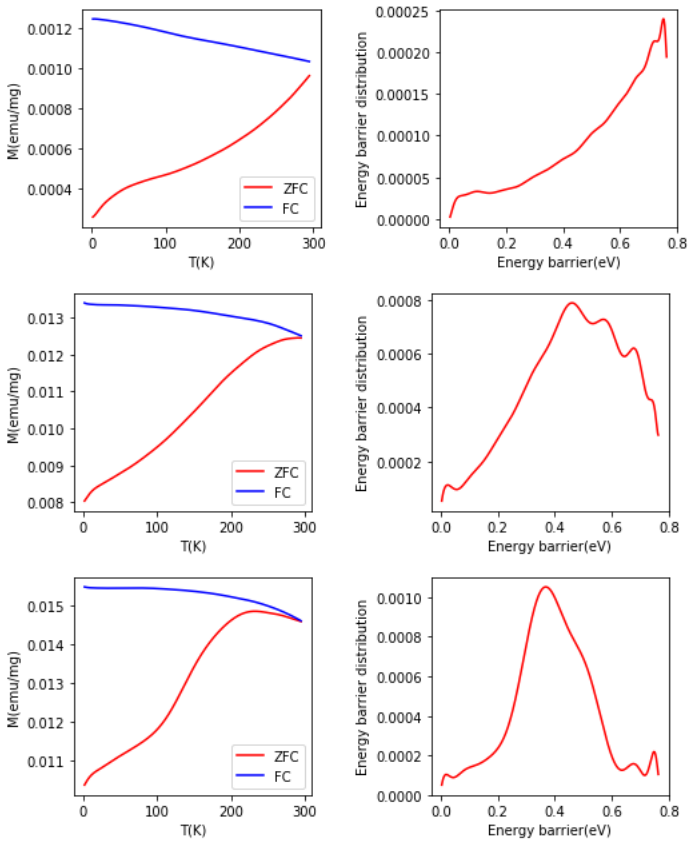

FIG. 4: Representation of the ZFC-FC(left) and barrier distribution (right) for 100 Oe (top) , 2000 Oe (middle) and 3000 Oe (bottom).

Two main maximums can be observed in ZFC revealing two main barrier distributions. The effect of the magnetic field in energy barriers is observable when the magnetic field is increased, producing a shift of the two maximums to lower temperatures due to the reduction of the energy barrier. At 5000 Oe the ZFC and FC curves overlap and they are completely reversible due to the barrier breakdown.

The barrier distributions at different applied fields are shown in figure 4 with their corresponding ZFC-FC curves. We can observe two main maxima, one at low temperatures and the other at higher temperatures. We can also observe that above 3000 Oe the first maximum disappears.

It is not possible to obtain the size distribution due to the sample do not present single domain particles. Nevertheless,this two energy barrier distributions may correspond to different anisotropies, different sizes or different compositions.

In order to find a physical interpretation of the two maximums in the ZFC curves and explain the origin of this two energy barrier distribution, we calculated the area under each maximum to know if it is due to the double particle size distribution or two different phases. The results are shown in figure 5. The ratio of two areas is approximately 1:9, which seems to be in accordance with the composition shown in figure 2. Nevertheless, it is not possible to confirm that this two energy barriers are related to the composition of the sample.

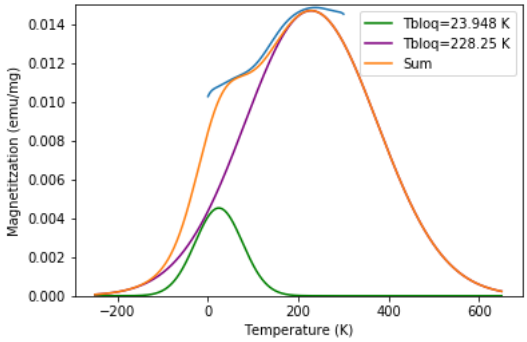

FIG. 5: Representation of the gaussian curves adjusted to the two maximums of ZFC curve at 3000 Oe.

C. Magnetic relaxation experiments

We also carried out magnetic relaxation experiments. We studied the evolution of magnetization with time when a saturating field applied to the system is turned off,at different temperatures. The magnetization presents a logarithmic dependence equation (4) with time if there is a energy barrier distribution. The magnetic viscosity can be extracted from the logarithmic decay dependence with time of magnetization moment. The results are exposed in figure 6.

Experimental data at 2-4K is not represented due to unfavourable fiability. The viscosity decreases monotonically as the temperature decreases, which is in good agreement with thermal relaxation . The presence of thermal relaxation at low temperatures is also supported by the fact that it is not possible to observe a change of slope in the representation of M vs $T\ln(t/t_0)$. Scaling with $T\ln(t/t_0)$ we can observe the collapse onto a single curve. In order to go deeper in the understanding

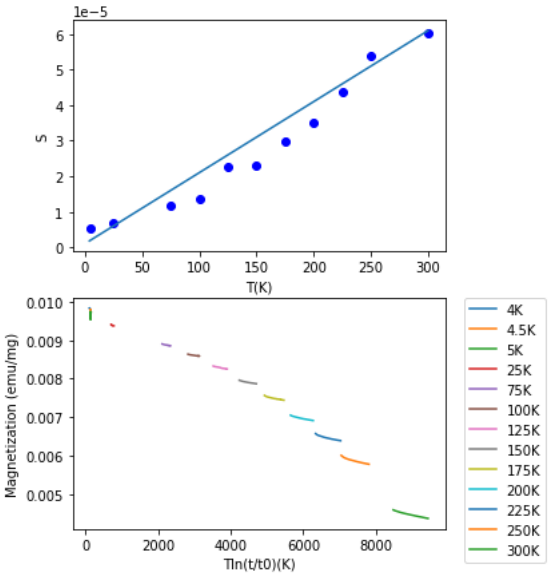

FIG. 6: Representation of the magnetic viscosity (top) and the magnetization versus $Tln(t/t_0)$ (bottom).

of the relaxation process, we performed magnetic relaxation measurements at low temperatures with a bigger field of 1000 Oe. Increasing the field, larger variations of magnetization are obtained, which means that resolution is improved. The magnetic viscosity and M vs $Tln(t/t_0)$ are shown in figure 7. In both cases , the scaling with $Tln(t/t_0)$ assemble nicely into the universal curve expected in the case of purely thermal relaxation.

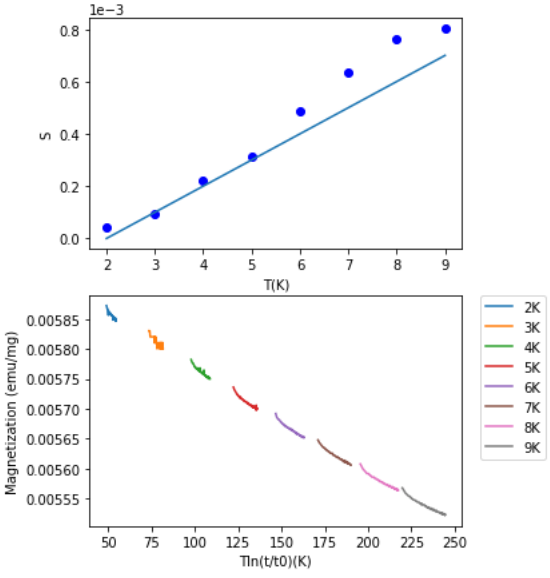

FIG. 7: Representation of the magnetic viscosity (above) and the magnetization versus $Tln(t/t_0)$ (bottom)

D. Susceptibility

Experimental curves of real and imaginary susceptibility are shown in figure 8 for a frequency of 10 Hz and 1000 Hz in figure 9 in the range 2-300K.

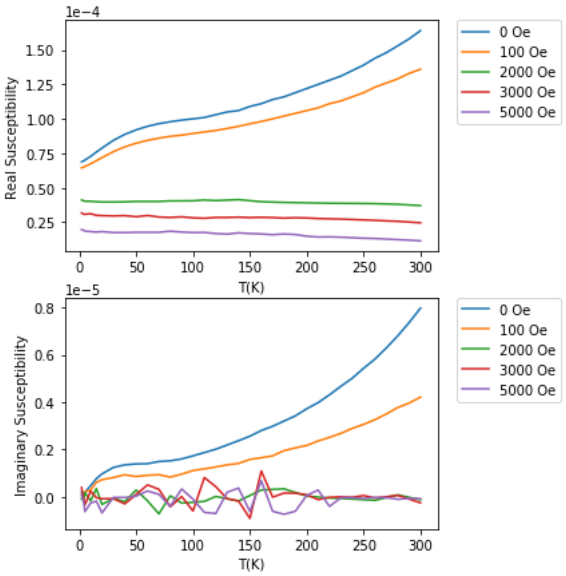

FIG. 8: Representation of the dependence on temperature of real susceptibility (above) and imaginary susceptibility (bottom) for a frequency of 10 Hz

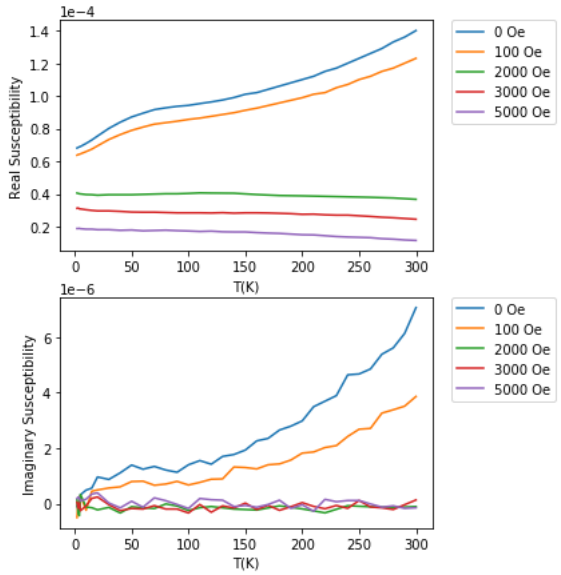

FIG. 9: Representation of the dependence on temperature of real susceptibility (above) and imaginary susceptibility (bottom) for a frequency of 1000 Hz

With no field applied and with a static field of 100 Oe we can observe an increasing behaviour of the two susceptibilities, in and out of phase for both frequencies. At

10 Hz the first maximum is not centered in the blocking temperature at 100 Oe due to the temperature blocking depend on the measurement frequency.On the other hand at 1000 Hz, the first maximum concurs with the blocking temperature at 100 Oe. The presence of a second maximum for both frequencies can be intuited at a blocking temperature higher than 300 K . The presence of this two maximums seems to be in accordance with ZFC curve at 100 Oe. This behaviour disappears as of 2000 Oe due to the magnetization cannot follow the alternating magnetic field, although the static field applied is lower than saturation field.

E. Permittivity

We also measure the electrical permittivity in a frequency range between 200 MHz and 20 GHz, for a volume of 5 mL of the sample and for different pressures applied.

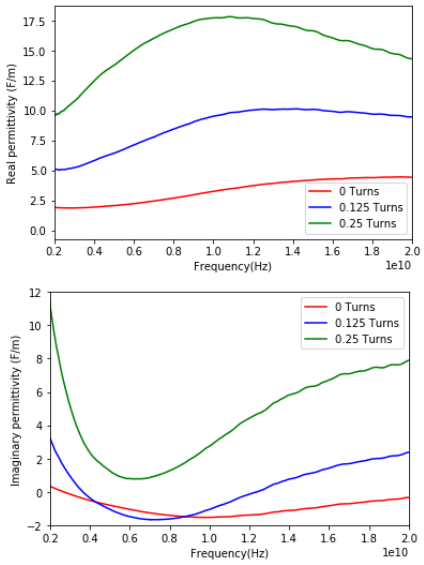

FIG. 10: Representation of the dependence on frequency of real permittivity (top) and imaginary permittivity(bottom)

The results are in good agreement with the fact that by increasing the pressure, we reduce the presence of air in the surface layers, so the permittivity increases because the air acts as a dielectric medium, which produces electric polarization when absorbs an electromagnetic wave. The real permittivity is related with charge storage and the imaginary part with losses, so it concurs with the fact that when real permittivity increases, imaginary diminishes. We can also observe that the main maximum in real permittivity is centered in a lower frequency when pressure increases. This implies that when the distance between particles is decreased due to the pressure, the maximum losses in permittivity shift to lower frequencies. The imaginary part shows negative values that may indicate that the calibration must be improved.

VI. CONCLUSIONS

The two main energy barrier distributions were obtained with ZFC curve at 3000 Oe. This is supported by the presence of hysteresis in M(H) , which suggest time dependent phenomena and energy barrier distribution. We cannot confirm that this two energy barrier distributions may correspond to different sizes or different compositions in the sample. Nevertheless, the area under the two maximums at a blocking temperature at ZFC in 3000 Oe seems to be in agreement with the composition of the sample. That would implied that the first maximum in ZFC may be related with iron nanoparticles due to the quantity of iron is approximately 10 % , so the magnetization is lower, and the second maximum may be related with the carbon media. Superparamagnetic behaviour at higher fields can also be observed in M(H) loops which may correspond to the Fe_3C and nanotubes . Moreover, thermal relaxation confirms the existence of energy barrier distributions. On the other hand, susceptibility measurements also suggest the presence of the two energy barrier distributions at lower fields than 2000 Oe. Due to the problems with calibration, we cannot confirm that the values of permittiviy are correct, although the shape of the curves may indicate also a maximum in real permittivity and the corresponding minimum in imaginary permittivity.

VII. ACKNOWLEDGEMENTS

I would like to express my sincere gratitude to my advisors Dr.Javier Tejada and Jamue Calvo, for their patience, motivation and immense knowledge. I also would to thank my dear friend , Kirn Kaur for being part of this work , and Joan Manel and Chao Chen for helping us in the laboratory.

I am also very thankfully for the support all these months of my parents, Eduard and Dolors and my dear partner Ricard.

[1] Iijima, *S. Helical microtubules of graphitic carbon*, Nature.354 (1991).

[2] Peter J.F. Harris, *Carbon nanotube science : synthesis, properties and applications* ,Cambridge U.Press (2009)

[3] Danilyuk, A.L. Prudnikava, A.L. Komissarov, Ivan Yanushkevich, K.I. Derory, Alain Le Normand, Francois Labunov, Vladimir Prischepa. *Interplay between exchange interaction and magnetic anisotropy for iron based nanoparticles in aligned carbon nanotube arrays* Vol.64 ,pp 337-345 (2014).